Journal of the Chinese Society of Mechanical Engineers, Vol.46, No.5, pp467~474 (2025)

Sol–Gel Derived SiO_2/PMMA Composite Coatings with Tunable Dispersion for Corrosion Protection of Ti-6Al-4V

Cheng-En Jiang*, Guan-Yu Chen* and Shih-Chen Shi**

Keywords：Silica nanoparticle; PMMA composite coating; Corrosion resistance

ABSTRACT

This study presents a sol–gel-based strategy to synthesize amorphous SiO_2 nanoparticles and incorporate them into PMMA to form corrosion-resistant composite coatings for Ti-6Al-4V substrates. The effects of synthesis parameters precursor concentration, catalyst concentration, reaction time, and temperature on particle size and dispersion were systematically investigated. Voronoi-based dispersion index ($D_{0.2}$) was used to quantify uniformity, showing that catalyst concentration played the most critical role in dispersion control. Well-dispersed SiO_2 nanoparticles ($D_{0.2}$ > 50%) significantly improved electrochemical barrier performance, as confirmed by electrochemical impedance spectroscopy (EIS). The optimal composite, containing 5 wt% SiO_2, exhibited impedance magnitudes in the range of 10^8–10^9 Ω·cm² at low frequencies and stable phase angles (80–90°), indicating dense coating morphology and strong dielectric behavior. In contrast, higher filler content (10 wt%) led to aggregation, structural defects, and diminished corrosion protection. The findings confirm that nanoparticle dispersion is a key factor in coating integrity and validate a practical design route for high-performance polymer-based anticorrosion coatings.

INTRODUCTION

Total Joint Replacement is a cornerstone of modern orthopedic surgery, providing practical and long-term solutions for patients with advanced joint diseases such as osteoarthritis and rheumatoid arthritis. With clinical success rates exceeding 99%, TJR procedures are widely adopted in aging populations. However, long-term implant performance is often hindered by material degradation, wear, and especially corrosion, which is accelerated by exposure to body fluids. Developing surface coatings with improved biocompatibility and corrosion resistance is essential to extend implant lifespan and reduce failure rates.

Polymeric biomaterials play a critical role in medical applications due to their structural similarity to biological tissues, mechanical durability, and ease of processing (Shi & Huang, 2018). Among them, poly(methyl methacrylate) (PMMA) is widely used for biocompatibility. However, its corrosion resistance is limited by polar functional groups (Song et al., 2020) that interact with water and ions. Studies indicate that incorporating fillers into films can significantly enhance their mechanical properties and barrier capabilities (Chou et al., 2021; Shi et al., 2020).
Organic additives have also been employed to enhance the properties of PMMA-based composites effectively (Shi et al., 2022).

Titanium alloys, especially Ti-6Al-4V, are commonly used in implants due to their high strength-to-weight ratio and biocompatibility. However, previous studies have reported that prolonged implantation releases Al and V ions, especially V, which are potentially toxic (Luo et al., 2013). These alloys also exhibit poor tribological behavior, including high friction coefficients and low wear resistance (Budzynski et al., 2006), and are prone to corrosion in physiological environments.

This study, SiO_2 nanoparticles were synthesized via sol–gel processing and introduced into PMMA matrices (Morales-Acosta et al., 2013; Rahman & Padavettan, 2012; Singh et al., 2014; Yang & Nelson, 2004). Dispersion quality was quantified using the ($D_{0.2}$) metric and Voronoi diagram analysis (Alvarado-Rivera et al., 2007; Erwig, 2000). EIS results showed that coatings with well-dispersed SiO_2 exhibited high impedance values at low frequencies (|Z| ~10^8–10^9 Ω·cm²). They retained high phase angles, indicating

Paper Received May, 2025. Revised July, 2025. Accepted August, 2025. Author for Correspondence: Shih-Chen Shi.

* *Student, Department of Mechanical Engineering, National Cheng Kung University, 70101 Tainan, Taiwan*

** *Professor, Department of Mechanical Engineering, National Cheng Kung University, 70101 Tainan, Taiwan*

strong dielectric behavior and excellent corrosion protection, as shown in Fig. 1.

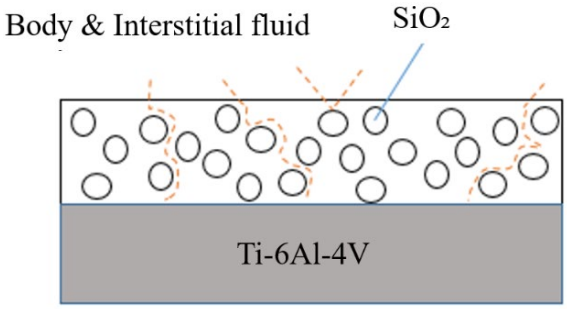

Fig. 1 Schematic illustration of the barrier effect of dispersed nanoparticles in reducing the permeation of corrosive agents.

MATERIALS PREPARATION AND EXPERIMENTAL PROCEDURE

Materials

This study used a PMMA/SiO_2 composite system composed of organic and inorganic components. The organic phase included poly(methyl methacrylate) (PMMA, Sigma-Aldrich) as the polymer matrix, tetrahydrofuran (THF, Reagents Duksan) as the solvent, benzoyl peroxide (BPO, Alfa Aesar) as the thermal initiator, and 3-(trimethoxysilyl)propyl methacrylate (MPTS, Sigma-Aldrich) as a silane coupling agent to enhance interfacial adhesion between the polymer and inorganic phase. These materials were combined to ensure structural integrity and compatibility within the composite matrix. As the silica precursor, the inorganic phase comprised tetraethyl orthosilicate (TEOS, Thermo Scientific). Deionized water and ethanol (SHIN-SHIN CHEMICAL CO.) were co-solvents to facilitate hydrolysis and condensation reactions. At the same time, ammonia (NH_3, PanReac AppliChem) was used as a sol–gel synthesis catalyst. All chemicals were used without additional purification to ensure experimental reproducibility and consistency. This formulation enabled controlled integration of silica nanoparticles into the PMMA matrix through sol–gel processing. The resulting composite structure was the basis for corrosion-resistant coatings evaluated in this study. Further optimization of reaction conditions was performed to regulate particle dispersion and ensure coating uniformity.

Sol–Gel Synthesis of SiO_2 Nanoparticles

Silica (SiO_2) nanoparticles were synthesized via the sol–gel method using tetraethyl orthosilicate (TEOS) as the precursor. Ethanol, deionized water, and aqueous ammonia (NH_3(aq)) served as the co-solvent, hydrolysis medium, and catalyst, respectively. This approach enabled the formation of fine silica particles under mild reaction conditions. The Taguchi experimental design was applied to optimize synthesis for improved dispersion (Roy, 2010). Four control factors were selected: TEOS concentration, ammonia concentration, reaction temperature, and reaction time. Each factor was tested at three levels.

Nine experimental conditions were assigned using an L_9 orthogonal array. The design matrix is shown in Table 1, and the experimental runs are listed in Table 2.

This systematic approach identified optimal parameters for well-dispersed nanoparticles.

Table 1. Control factors and levels used in Taguchi design.

Factor	1	2	3	4
Level	TEOS (wt%)	$NH_{3(aq)}$ (M)	Temp (°C)	Time (min)
1	5	0.01	20	90
2	7	0.05	40	180
3	10	0.1	60	270

Table 2. Experimental conditions based on the L_9 orthogonal array.

Sample	Code Name
5 wt%+0.01 M+20°C +90 min	P5N012090
5 wt%+0.05 M+40°C +180 min	P5N0540180
5 wt%+0.1 M+60°C +270 min	P5N160270
7 wt%+0.01 M+40°C +270 min	P7N0140270
7 wt%+0.05 M+60°C +90 min	P7N056090
7 wt%+0.1 M+20°C +180 min	P7N120180
10 wt%+0.01 M+60°C +180 min	P10N0160180
10 wt%+0.05 M+20°C +270 min	P10N0520270
10 wt%+0.1 M+40°C +90 min	P10N14090

Silica nanoparticles were synthesized via a sol–gel method with a molar ratio of TEOS: Ethanol: deionized water = 1:2:4. Ethanol was first added to TEOS to initiate alcoholysis, followed by magnetic stirring at room temperature. Aqueous ammonia was then introduced as the catalyst based on the experimental design. Deionized water was slowly added dropwise to prevent premature silica aggregation. The solution was gradually heated to the target reaction temperature and sealed for the designated duration. This controlled process minimized particle agglomeration during nucleation.

Preparation of PMMA/SiO_2 Composites

The dispersion of silica nanoparticles plays a critical role in determining the performance of PMMA-based composites. While uniform dispersion maximizes reinforcement efficiency, the high specific surface area of nanoparticles often leads to aggregation, limiting their effectiveness. To overcome this, the sol–gel process was carried out under alkaline conditions (pH = 7–11), where negatively charged silica surfaces promote electrostatic repulsion and reduce particle clustering. Furthermore, to improve interfacial compatibility between the hydrophilic SiO_2 and hydrophobic PMMA matrix, the coupling agent MPTS

was introduced. MPTS possesses a methacrylate group that co-polymerizes with PMMA and a silane group that bonds with silica. Using BPO as an initiator, grafting of MPTS onto the PMMA chains was achieved, allowing subsequent covalent attachment to SiO_2. The reaction mechanism is illustrated in Fig. 2.

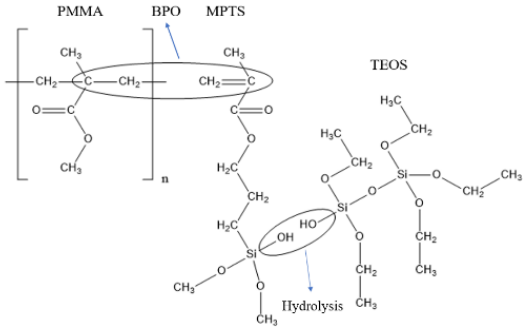

Fig. 2 Interaction Mechanism of MPTS Coupling Agent Between Organic Phase (PMMA) and Inorganic Phase (TEOS)

PMMA/SiO_2 composite coatings were prepared by dispersing silica nanoparticles into a PMMA matrix. PMMA powder was dissolved in tetrahydrofuran (THF) at 40 °C (weight ratio 1:5), then cooled before adding benzoyl peroxide (BPO) and MPTS (molar ratio MPTS:TEOS: BPO = 1:2:0.01). The inorganic phase was synthesized via sol–gel using TEOS, Ethanol, deionized water, and ammonia (1:2:4) under 400 rpm stirring. The sol was slowly added to the organic phase and stirred for 1 hour to ensure uniform dispersion. Degassing was performed at 40 °C using a rotary evaporator to remove bubbles and residual solvent. Afterward, 20 mL of the mixture was poured into clean Petri dishes, covered with foil, air-dried, and oven-dried at 60 °C for 24 hours. The resulting solid films were laser-cut into standard sizes for structural and electrochemical testing.

SiO_2 Particle Size Analysis

In this study, the particle size of nanofillers was analyzed using ImageJ, an open-source image processing software developed by the National Institutes of Health (NIH, USA). The software provides robust tools for quantitative particle analysis based on image data. Specifically, the "Analyze Particles" function was utilized to extract key morphological parameters, including particle count, projected area, perimeter, bounding rectangle dimensions (width and height), major and minor axes of the best-fit ellipse, and Feret's diameter.

Feret's diameter refers to the longest distance between two parallel tangents on opposite sides of the particle's outline, representing its maximum dimension. the Feret's diameter is particularly suitable for characterizing irregular or rough-edged convex particles, such as those commonly encountered in sol–gel derived nanomaterial (Igathinathane et al., 2009).

The analysis procedure included image calibration, particle segmentation using the Weka plugin, binary conversion, and hole filling. Valid particles were selected using the Wand tool, followed by parameter extraction such as Feret diameter and projected area through the "Analyze Particles" function. The average Feret diameter was ultimately adopted as the representative particle size. The complete analysis workflow is illustrated in Fig. 3 (a)–(f).

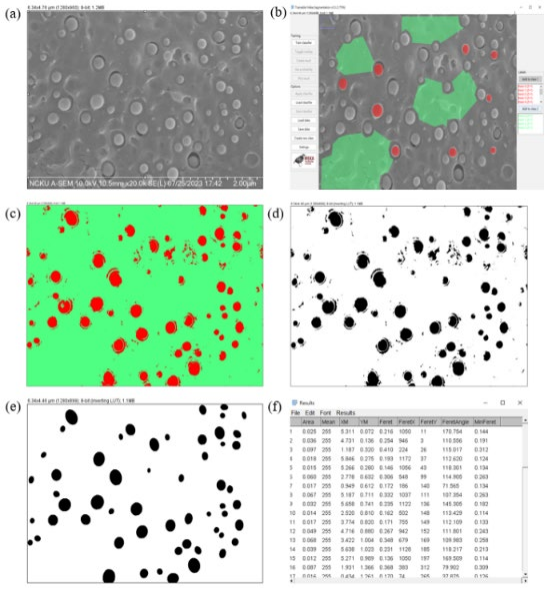

Fig. 3 SiO_2 nanoparticle size analysis workflow using ImageJ. (a) Set scale; (b) Weka segmentation; (c) Binarization and hole filling; (d) Particle selection with Wand tool; (e) Analyze particles; (f) Output results.

Particle Dispersion Analysis and Statistical Processing

To quantitatively evaluate the dispersion of SiO_2 nanoparticles in the composite matrix, scanning electron microscopy (SEM) was employed to capture high-resolution images of the filler distribution. The acquired images were binarized and processed using the Voronoi diagram function in ImageJ to perform particle segmentation and region partitioning. Each particle on the 2D plane was localized, and lines were drawn between neighboring particles. Perpendicular bisectors of these lines were then constructed to define the boundaries of Voronoi cells, resulting in a tessellation of non-overlapping polygons that assigned a unique area to each particle, as shown in Fig. 4 (a)–(f).

Following segmentation, the area of each Voronoi cell was calculated and used to generate a histogram, which was then fitted with a normal distribution curve. Based on this statistical distribution, a dispersion parameter D_k was defined, representing the proportion of particles whose associated areas fall

within the range of the mean value μ±k%. A higher D_k indicates a greater number of particles with areas close to the mean, thereby suggesting a more uniform and well-dispersed filler distribution.
This semi-automated approach enables objective and reproducible analysis of particle spacing and dispersion uniformity across different sample conditions. The mathematical expression for D_k is given by:

$$D_k = \int_{\mu(1-k)}^{\mu(1+k)} f(a)da \qquad (1)$$

where $f(a)$ denotes the probability density function of the Voronoi cell area distribution, μ is the mean area, and k is the tolerance range expressed as a percentage of the mean.

The dispersion of nanoparticles was quantified using the $D_{0.2}$ index, which represents the probability of finding particles within ±20% of the average particle-associated area. This index reflects the proportion of particles whose corresponding Voronoi cell areas fall within a defined range centered around the mean. A higher $D_{0.2}$ value indicates a narrower distribution and thus a more uniform dispersion of particles within the composite matrix.

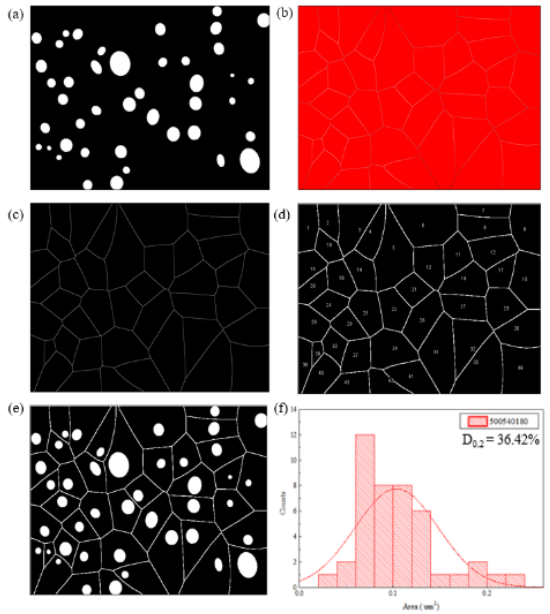

Fig. 4 SiO_2 particle dispersion analysis workflow: (a) Voronoi diagram generation; (b) threshold adjustment; (c) measurement setup; (d, e) particle segmentation; (f) statistical output of particle distribution

Corrosion Resistance Test

Electrochemical impedance spectroscopy (EIS) was employed to evaluate the corrosion resistance of PMMA/SiO_2 composite coatings on Ti-6Al-4V substrates. While in the gel state, the composite solution was uniformly applied to the pretreated Ti-6Al-4V surface using a film applicator, ensuring a coating thickness of approximately 5 μm, as shown in Fig. 5 (a).

This method allowed consistent surface coverage suitable for electrochemical testing. After drying and curing, the coated samples were tested using a three-electrode EIS system. Impedance data were collected over a frequency range to analyze coating performance against corrosion. The results provided insight into barrier properties and interfacial behavior. The measured impedance characteristics were a basis for evaluating how nanoparticle dispersion influenced corrosion protection. This result enabled a quantifiable comparison among samples with different SiO_2 distributions.

EIS was used to assess the corrosion behavior of PMMA/SiO_2 coatings on Ti-6Al-4V. Samples were mounted in a reaction cell Fig. 5 (b), with conductive copper tape on the back and 1 cm^2 of the coated surface exposed to a 3.5 wt.% NaCl solution. Before measurement, samples were immersed for 10 minutes to stabilize the open circuit potential (OCP). A three-electrode setup was used: platinum as counter, saturated calomel electrode (SCE) as reference, and the coated sample as working electrode. Impedance data were collected from 100 kHz to 0.01 Hz using a 0.2 V sine wave, with 8 readings averaged per frequency point. Potentiodynamic polarization tests were also conducted with a scan range of OCP ±1.5 V and a scan rate of 0.002 V/s, following a 10 minute OCP hold.

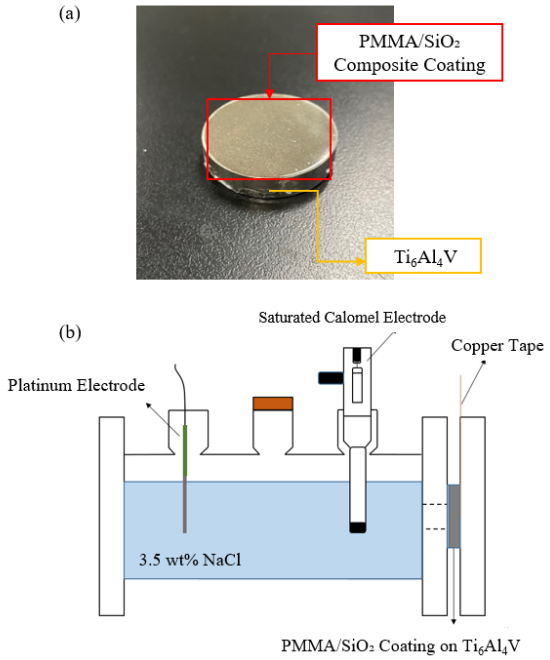

Fig. 5 (a) Coating application on Ti-6Al-4V substrate using a film applicator. (b). Schematic of the electrochemical cell setup used for EIS and polarization tests.

RESULTS AND DISCUSSION

Optimization of Silica Synthesis Parameters

A four-factor, three-level Taguchi design synthesizes silica nanoparticles, resulting in nine test groups and one validation group. The four parameters included TEOS concentration, NH_3(aq) concentration, reaction temperature, and time. Table 3 shows the orthogonal array, while signal-to-noise (S/N) ratios and ANOVA results are summarized in Table 4 and Table 5 using the dispersion index $D_{0.2}$. Results showed NH_3(aq) concentration had the most significant influence on dispersion (63.25%), followed by TEOS concentration (21.81%), temperature (13.50%), and time (1.45%). This result indicated that catalyst content was the dominant factor for uniform particle distribution. According to the S/N response in Fig. 6, the optimal synthesis condition was TEOS 5 wt%, NH_3 0.1 M, 60 °C, and 180 min, corresponding to sample P5N160180V.

Table 3. The experimental design matrix is based on the Taguchi L_9 array.

No.	wt%	$NH_{3(aq)}$	Temp	Time	$D_{0.2}$	S/N
1	5	0.01	20	90	23.96	27.59
2	5	0.05	40	180	36.42	31.23
3	5	0.1	60	270	51.63	34.26
4	7	0.01	40	270	20.53	26.25
5	7	0.05	60	90	30.44	29.67
6	7	0.1	20	180	32.32	30.19
7	10	0.01	60	180	31.09	29.85
8	10	0.05	20	270	32.45	30.22
9	10	0.1	40	90	40.33	32.11

Table 4. Mean $D_{0.2}$ values under different factor levels

Factor	Level 1	Level 2	Level 3
wt %	31.02	28.70	30.73
NH_3	27.90	30.37	32.19
Temp	29.33	29.86	31.26
Time	29.79	30.42	30.24

Table 5. ANOVA summary for $D_{0.2}$

Factor	DOF	SS	MS	Contribution (%)
wt %	2	9.59	4.80	21.81
NH_3	2	27.83	13.97	63.25
Temp	2	5.94	2.97	13.50
Time	2	0.64	0.32	1.45

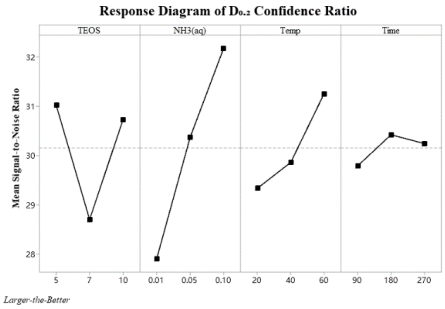

Fig. 6 Response diagram of $D_{0.2}$ confidence ratio

FTIR Analysis of the PMMA/SiO_2 Composite Structure

Raman spectroscopy was used to examine the structural effects of different SiO_2 loadings in PMMA/SiO_2 composites. Fig. 7 shows spectra for pure PMMA and composites with 5, 7, and 10 wt% SiO_2, used to confirm silica presence and analyze bonding behavior. As SiO_2 content increased, the intensity of PMMA peaks at 1450, 1640, and 1758 cm^{-1} also increased, suggesting enhanced chain ordering and polymerization, likely due to better nanoparticle dispersion.

In contrast, SiO_2 peaks at 460 and 711 cm^{-1} weakened, possibly due to polymer coverage or silica restructuring. Stronger signals in the 986–1048 cm^{-1} range indicated possible Si–OH or Si–O–C bond formation, supporting chemical bonding between organic and inorganic phases rather than simple physical mixing.

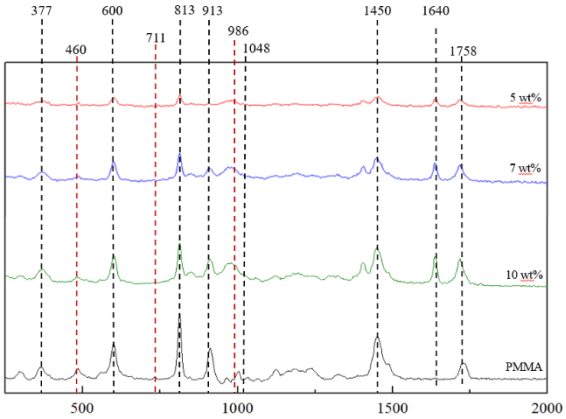

Fig. 7 Raman spectra of PMMA/SiO_2 composites with different silica contents.

Statistical Analysis of SiO_2 Particle Dispersion

SEM images taken at 30.0k magnification with a 1.00 µm scale were binarized and processed using ImageJ to construct Voronoi diagrams, as shown in Fig. 8. The area of each Voronoi cell was measured and used to create histograms with normal distribution fits, illustrated in Fig. 9. The $D_{0.2}$ index, defined as the percentage of areas within ±20% of the mean, was calculated to quantify particle dispersion. Table 6 summarizes the particle size and $D_{0.2}$ values across different synthesis conditions. Higher TEOS concentrations (10 wt%) increased particle size from 100–200 nm to 300–400 nm. Longer reaction times led to greater aggregation, while elevated temperatures enhanced nucleation and suppressed clustering. Ammonia concentration plays a key role in dispersion. At 0.1 M, weak repulsive forces allow particles to agglomerate, reducing $D_{0.2}$ to 51.63%. In contrast, optimal dispersion ($D_{0.2}$ >70%) occurs at 5 wt% TEOS and 0.01 M NH_3, where particles are more uniformly

distributed.

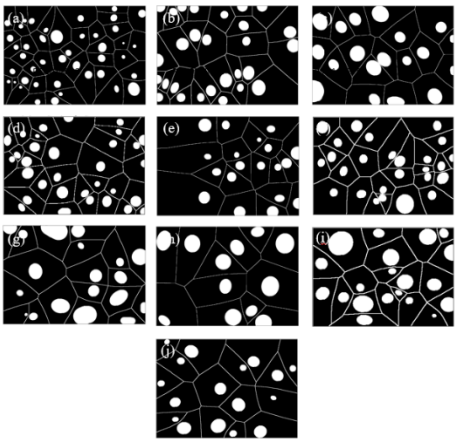

Fig. 8 SEM-based Voronoi diagrams of SiO_2 particle distributions.

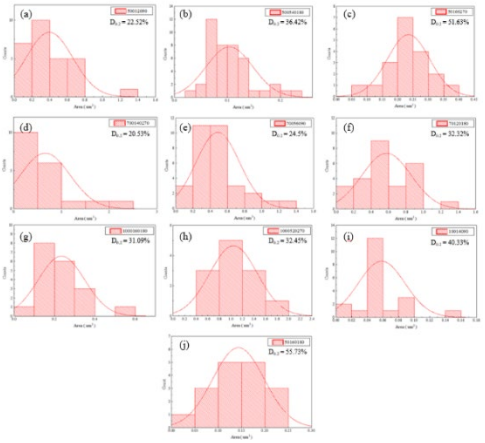

Fig. 9 Histogram and regular distribution of Voronoi region areas.

Table 6 Particle size and dispersion index ($D_{0.2}$) under various conditions.

No.	Code Name	$D_{0.2}$(%)	Average particle size (nm)
1	P5N012090	22.52	118
2	P5N0540180	36.42	156
3	P5N160270	51.63	204
4	P7N0140270	20.53	260
5	P7N056090	24.5	200
6	P7N120180	32.32	238
7	P10N0160180	31.09	339
8	P10N0520270	32.45	435
9	P10N14090	40.33	332
10	P5N160180V	55.73	148

Electrochemical Impedance Analysis

Incorporating fillers into the film leads to a denser and more uniform substrate structure with reduced porosity , while the fillers themselves can effectively extend the diffusion path of moisture or corrosive agents within the nanocomposite coating (Chou et al., 2021; Rahmadiawan et al., 2024; Shi et al., 2025). To evaluate the corrosion resistance of the PMMA/SiO_2 coatings, electrochemical impedance spectroscopy (EIS) was conducted. Impedance magnitude (|Z|) and phase angle (θ) in Fig. 10 (a) and (b), respectively, indicated the coatings' barrier performance and dielectric behavior. High |Z| values at low frequencies (<1 Hz) suggest strong resistance to ion penetration, while θ values near 90° indicate ideal capacitive behavior and coating integrity. As shown in Fig. 10 (a), the sample containing 5 wt% SiO_2 with a $D_{0.2}$ dispersion index of 55.73% exhibited the highest impedance modulus, ranging from 10^8 to 10^9 Ω·cm², indicating superior corrosion protection performance. In contrast, the 10 wt% sample showed reduced impedance (10^5–10^6 Ω·cm²), likely due to particle agglomeration and structural defects. Fig. 10 (b) shows that 5 wt% and 7 wt% samples maintained θ between 80–90° at mid-high frequencies, while 10 wt% samples dropped below 40°, indicating compromised dielectric performance.

Fig. 11 presents the correlation between $D_{0.2}$ and charge transfer resistance (Rct) at different SiO_2 contents. As shown in Table 7, the first entry corresponds to the pure PMMA coating, which served as the control group in this study. An increasing trend in Rct values was observed with higher $D_{0.2}$ dispersion indices. The 5 wt% SiO_2 sample exhibited the highest performance, with an Rct value reaching 8.11 × 10^8 Ω·cm². This result confirms that improved nanoparticle dispersion contributes to the formation of a dense and continuous protective barrier, thereby significantly enhancing the corrosion resistance of the coating.

The impedance magnitude and phase angle results confirmed that the PMMA/SiO_2 composite coating exhibited excellent electrochemical resistance when SiO_2 was well dispersed at a loading of 5 wt%. High SiO_2 content led to particle agglomeration and structural defects, which reduced the coating's corrosion resistance. These findings support the interpretation that particle dispersion is the key factor governing the corrosion protection performance of PMMA/SiO_2 composites.

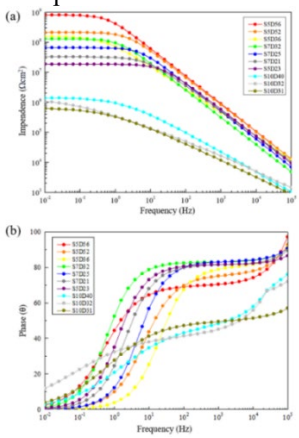

Fig. 10 EIS results of PMMA/SiO_2 coatings: (a) impedance vs. frequency; (b) phase angle vs. frequency.

Table 7 Summary of $D_{0.2}$ and Rct values for each sample.

Code Name	$D_{0.2}$ (%)	R_{ct} ($\Omega \cdot cm^2$)
PMMA		1.13×10^5
P5N012090	22.52	1.87×10^7
P5N0540180	36.42	1.55×10^8
P5N160270	51.63	2.15×10^8
P5N012090	55.73	8.11×10^8
P7N0140270	20.53	3.28×10^7
P7N056090	24.5	6.62×10^7
P7N120180	32.32	1.30×10^8
P10N0160180	31.09	8.42×10^5
P10N0520270	32.45	1.81×10^6
P10N14090	40.33	3.32×10^6

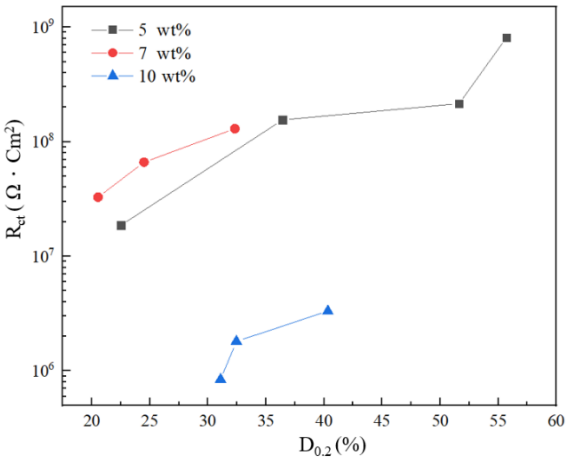

Fig. 11 Correlation between $D_{0.2}$ and charge transfer resistance at different SiO_2 content

CONCLUSIONS

This study successfully synthesized amorphous SiO_2 nanoparticles via the sol–gel method and incorporated them into PMMA to fabricate composite coatings.

EDS analysis confirmed a Si:O atomic ratio near the theoretical 1:2 value, and Raman spectroscopy verified the presence of silica and its integration into the PMMA matrix. As TEOS concentration increased, the intensity of silica-related Raman peaks also rose, indicating chemical interaction between the organic and inorganic phases.

Both particle size and dispersion were effectively controlled by tuning precursor and catalyst concentrations, reaction time, and temperature. While precursor concentration, time, and temperature primarily affected particle growth, catalyst concentration was the dominant factor influencing dispersion.

Voronoi-based $D_{0.2}$ analysis showed most samples had dispersion indices above 30%, confirming that the sol–gel route effectively limited agglomeration under appropriate conditions.

Electrochemical impedance spectroscopy demonstrated that coatings with higher $D_{0.2}$ values provided greater corrosion resistance.

Poor dispersion led to particle clustering and defect pathways, which allowed water penetration and weakened barrier integrity. In contrast, coatings with 5 wt% SiO_2 and good dispersion ($D_{0.2}$ > 50%) exhibited high impedance and stable phase behavior, indicating superior protection performance. In conclusion, well-dispersed SiO_2 nanoparticles play a critical role in enhancing the corrosion resistance of PMMA coatings on Ti-6Al-4V substrates.

Although this study systematically investigated the effects of TEOS concentration, reaction temperature, and reaction time on the sol–gel synthesis of SiO_2, precise control over nanoparticle size remained challenging due to strong interdependencies among these parameters. Higher TEOS concentrations increased nucleation density and reduced particle residence time, resulting in larger particles. Elevated temperatures accelerated nucleation but suppressed particle growth, producing smaller sizes. Longer reaction times promoted aggregation, leading to larger particles. Moreover, the dynamic growth and aggregation behavior intrinsic to the sol–gel system, especially before full TEOS conversion, contributed to size variability even under fixed conditions.

The study focuses on the dispersion behavior of SiO_2 nanoparticles within PMMA composite coatings and their influence on corrosion resistance. The results demonstrate that uniform dispersion of SiO_2 significantly enhances the barrier properties and electrochemical stability of the coating. However, this study has not yet systematically explored the mechanical performance and tribological behavior of the material. Future research will extend to evaluating mechanical properties including hardness, tensile strength, and wear resistance, in order to establish a more comprehensive framework for material performance assessment and to enhance the practical applicability and design reliability of composite coatings.

ACKNOWLEDGMENT

This work was supported by the National Science and Technology Council (NSTC), Taiwan (Grant Nos. 112-2221-E-006-173, 113-2221-E-006-087-MY2, 113-2221-E-006-112-MY2, and 113-2221-E-006-116). The authors gratefully acknowledge the Core Facility Center at National Cheng Kung University, Taiwan, for providing access to the EM000600, funded by NSTC project 114-2740-M-006-001. Additional support from the Higher Education Sprout Project, Ministry of Education, Taiwan, through the Headquarters of University Advancement at National

Cheng Kung University (NCKU), is also gratefully acknowledged.

REFERENCES

Alvarado-Rivera, J., Muñoz-Saldaña, J., Castro-Beltrán, A., Quintero-Armenta, J., Almaral-Sánchez, J., & Ramírez-Bon, R. (2007). Hardness and wearing properties of SiO_2–PMMA hybrid coatings reinforced with Al_2O_3 nanowhiskers. physica status solidi c, 4(11), 4254-4259.

Budzynski, P., Youssef, A., & Sielanko, J. (2006). Surface modification of Ti–6Al–4V alloy by nitrogen ion implantation. Wear, 261(11-12), 1271-1276.

Chou, C.-T., Shi, S.-C., & Chen, C.-K. (2021). Sandwich-structured, hydrophobic, nanocellulose-reinforced polyvinyl alcohol as an alternative straw material. Polymers, 13(24), 4447.

Erwig, M. (2000). The graph Voronoi diagram with applications. Networks: An International Journal, 36(3), 156-163.

Harb, S. V., dos Santos, F. C., Pulcinelli, S. H., Santilli, C. V., Knowles, K. M., & Hammer, P. (2016). Protective coatings based on PMMA–silica nanocomposites reinforced with carbon nanotubes. Carbon nanotubes–current progress of their polymer composites. 1st ed. Rijeka, Croatia: Intech, 195-225.

Harb, S. V., Trentin, A., Uvida, M. C., Magnani, M., Pulcinelli, S. H., Santilli, C. V., & Hammer, P. (2020). A comparative study on PMMA-TiO_2 and PMMA-ZrO_2 protective coatings. Progress in Organic Coatings, 140, 105477.

Igathinathane, C., Pordesimo, L., Columbus, E. P., Batchelor, W. D., & Sokhansanj, S. (2009). Sieveless particle size distribution analysis of particulate materials through computer vision. Computers and Electronics in Agriculture, 66(2), 147-158.

Kumar, A. M., Latthe, S. S., Sudhagar, P., Obot, I., & Gasem, Z. M. (2015). In-situ synthesis of hydrophobic SiO_2-PMMA composite for surface protective coatings: experimental and quantum chemical analysis. Polymer, 77, 79-86.

Luo, Y., Yang, L., & Tian, M. (2013). Application of biomedical-grade titanium alloys in trabecular bone and artificial joints. In Biomaterials and medical tribology (pp. 181-216). Elsevier.

Morales-Acosta, M., Alvarado-Beltrán, C., Quevedo-López, M., Gnade, B., Mendoza-Galván, A., & Ramírez-Bon, R. (2013). Adjustable structural, optical and dielectric characteristics in sol–gel PMMA–SiO_2 hybrid films. Journal of Non-Crystalline Solids, 362, 124-135.

Rahmadiawan, D., Shi, S.-C., Abral, H., Ilham, M. K., Sugiarti, E., Muslimin, A. N., Ilyas, R., Lapisa, R., & Putra, N. S. D. (2024). Comparative analysis of the influence of different preparation methods on the properties of TEMPO-oxidized bacterial cellulose powder films. Journal of Natural Fibers, 21(1), 2301386.

Rahman, I. A., & Padavettan, V. (2012). Synthesis of silica nanoparticles by sol-gel: size-dependent properties, surface modification, and applications in silica-polymer nanocomposites—a review. Journal of nanomaterials, 2012(1), 132424.

Roy, R. K. (2010). A primer on the Taguchi method. Society of manufacturing engineers.

Shi, S.-C., Chen, T.-H., & Mandal, P. K. (2020). Enhancing the mechanical and tribological properties of cellulose nanocomposites with aluminum nanoadditives. Polymers, 12(6), 1246.

Shi, S.-C., & Huang, T.-F. (2018). Effects of temperature and humidity on self-healing behaviour of biopolymer hydroxylpropyl methylcellulose for ecotribology. Surface and Coatings Technology, 350, 997-1002.

Shi, S.-C., & Zeng, X.-X. (2022). Effect of the strengthening mechanism of SiO_2 reinforced poly (methyl methacrylate) on ductility performance. Journal of Polymer Research, 29(10), 408.

Shi, S. C., Lin, C.-F., Liu, C.-F., & Chen, T.-H. (2022). Tribological and mechanical properties of cellulose/PMMA composite. Polymers and Polymer Composites, 30, 09673911221140935. https://doi.org/https://doi.org/10.1177/09673911221140935

Shi, S.-C., Rao, H.-W., & Rahmadiawan, D. (2025). Enhanced optical measurement and stress quantification of film roll wrinkling in roll-to-roll processing. Journal of the Chinese Society of Mechanical Engineers, 46(3), 223–231.

Singh, L. P., Bhattacharyya, S. K., Kumar, R., Mishra, G., Sharma, U., Singh, G., & Ahalawat, S. (2014). Sol-Gel processing of silica nanoparticles and their applications. Advances in colloid and interface science, 214, 17-37.

Song, J., Winkeljann, B., & Lieleg, O. (2020). Biopolymer-based coatings: promising strategies to improve the biocompatibility and functionality of materials used in biomedical engineering. Advanced Materials Interfaces, 7(17), 2000850.

Yang, F., & Nelson, G. L. (2004). PMMA/silica nanocomposite studies: synthesis and properties. Journal of applied polymer science, 91(6), 3844-3850.